

**Computer simulations show that Neanderthal facial morphology represents adaptation to cold and high energy demands, but not heavy biting**

Journal:	<i>Proceedings B</i>
Manuscript ID	RSPB-2018-0085.R1
Article Type:	Research
Date Submitted by the Author:	11-Mar-2018
Complete List of Authors:	Wroe, Stephen; University of New England, Parr, William; University of New South Wales, School of Biological, Environmental and Earth Sciences Ledogar, Justin; University at Albany, Anthropology Bourke, Jason; University of New South Wales, Biological Earth and Environmental Science; Evans, Samuel; University of Newcastle, Mechanical Engineering Fiorenza, Luca; Monash University Benazzi, Stefano; Universita degli Studi di Bologna, Department of Cultural Heritage Hublin, Jean-Jacques; Max Planck Institute for Evolutionary Anthropology, Department of Human Evolution Stringer, Chris; Natural History Museum London, Kullmer, Ottmar; Senckenberg Research Institute, Department of Paleoanthropology and Messel Research Curry, Michael; University of New England Rae, Todd; Roehampton University, School of Health and Life Sciences Yokley, Todd; Metropolitan State University of Denver
Subject:	Evolution < BIOLOGY, Biomechanics < BIOLOGY
Keywords:	Neanderthal, Homo heidelbergensis, Computational Fluid Dynamics, Finite Element Analysis
Proceedings B category:	Palaeobiology

1 Computer simulations show that Neanderthal facial morphology  
2 represents adaptation to cold and high energy demands, but not heavy  
3 biting

4

5 Stephen Wroe<sup>1\*</sup>, William C. H. Parr<sup>2\*</sup>, Justin A. Ledogar<sup>1</sup>, Jason Bourke<sup>3</sup>, Samuel P. Evans<sup>4</sup>, Luca Fiorenza<sup>5</sup>, Stefano Benazzi<sup>6,7</sup>, Jean-  
6 Jacques Hublin<sup>7</sup>, Chris Stringer<sup>8</sup>, Ottmar Kullmer<sup>9</sup>, Michael Curry<sup>1</sup>, Todd C. Rae<sup>10</sup>, & Todd R. Yokley<sup>11</sup>

7

8 <sup>1</sup>Function, Evolution & Anatomy Research Lab, School of Environmental & Rural Science, University of New England, NSW, 2351,

9 <sup>2</sup>Surgical and Orthopaedic Research Laboratory (SORL), Level 1, Clinical Sciences Bld, Gate 6, Prince of Wales Clinical School, University of  
10 New South Wales (UNSW), Avoca St, Randwick, Sydney, NSW 2031, Australia

11 <sup>3</sup>Department of Biological Sciences, North Carolina State University, Athens, Ohio, USA

12 <sup>4</sup>School of Engineering, University of Newcastle, Callaghan, NSW, 2308, Australia

13 <sup>5</sup>Department of Anatomy and Developmental Biology, Monash University, Clayton, Victoria, 3800, Australia

14 <sup>6</sup>Department of Cultural Heritage, University of Bologna, Via degli Ariani 1, Ravenna, 48121, Italy

15 <sup>7</sup>Department of Human Evolution, Max Planck Institute for Evolutionary Anthropology, 04103 Leipzig, Germany

16 <sup>8</sup>Department of Earth Sciences, Natural History Museum, London SW7 5BD, UK

17 <sup>9</sup>Senckenberg Forschungsinstitut Frankfurt am Main, Abteilung Paläoanthropologie und Messelforschung, Sektion Tertiäre Säugetiere,  
18 Senckenberganlage 25, 60325 Frankfurt am Main, Germany

19 <sup>10</sup>Centre for Research in Evolutionary and Environmental Anthropology, University of Roehampton, London, UK

20 <sup>11</sup>Metropolitan State University of Denver, P.O. Box 173362, Campus Box 28, Denver, CO 80217-3362, USA

21

22 \*These authors contributed equally to this work.

23

24 **Three adaptive hypotheses have been forwarded to explain the distinctive Neanderthal face: 1) an improved ability to**  
25 **accommodate high anterior bite forces, 2) more effective conditioning of cold and/or dry air, and, 3) adaptation to**  
26 **facilitate greater ventilatory demands. We test these hypotheses using three-dimensional models of Neanderthals,**  
27 **modern humans, and a close outgroup (*H. heidelbergensis*), applying finite element analysis (FEA) and computational**  
28 **fluid dynamics (CFD). This is the most comprehensive application of either approach applied to date and the first to**  
29 **include both. FEA reveals few differences between *H. heidelbergensis*, modern humans and Neanderthals in their**  
30 **capacities to sustain high anterior tooth loadings. CFD shows that the nasal cavities of Neanderthals and especially**  
31 **modern humans condition air more efficiently than does that of *H. heidelbergensis*, suggesting that both evolved to**  
32 **better withstand cold and/or dry climates than less derived *Homo*. We further find that Neanderthals could move**  
33 **considerably more air through the nasal pathway than could *H. heidelbergensis* or modern humans, consistent with**  
34 **the propositions that, relative to our outgroup *Homo*, Neanderthal facial morphology evolved to reflect improved**

35 capacities to better condition cold, dry air, and, to move greater air volumes in response to higher energetic  
36 requirements.

37

38

### 39 **1. Introduction**

40 Neanderthals (*Homo neanderthalensis*) are an “archaic” human species which persisted through  
41 multiple glacial-interglacial cycles in mid-late Pleistocene Eurasia. A number of craniofacial features  
42 distinguish Neanderthals from modern humans, including a wide, tall nasal aperture, a depressed nasal  
43 floor, a wide projecting nasal bridge, a retro-molar gap, “swept back” zygomatic arches and a depressed  
44 nasal floor [1, 2]. Whether, or to what degree, some of these features may represent adaptations to  
45 heavy para-masticatory activity (teeth as tools), better conditioning of cold, dry air, increased ventilatory  
46 flows in response to higher energetic demands, genetic drift, or simply retained plesiomorphies shared  
47 with earlier *Homo* has been the subject of longstanding debate [3-5], but the Neanderthal cranium is  
48 certainly distinctive [6].

49 Of the three adaptive hypotheses offering explanations for Neanderthal craniofacial evolution, the  
50 anterior dental loading hypothesis (ADLH), suggesting that that the Neanderthal face incorporates  
51 adaptations to sustain high loads applied to the incisors and/or canines, is perhaps the oldest. It has  
52 been underpinned by evidence of heavy wear on the anterior teeth in Neanderthals, although  
53 comparable wear may exist among contemporaneous modern humans [7]. Early arguments for the  
54 ADLH theorised that the Neanderthal face was better able to oppose rotation under loading on the  
55 anterior teeth around either transverse [4] or sagittal [8] axes. A more nuanced interpretation has been  
56 that facial prognathism in Neanderthals represents a trade-off between demands for high bite force at  
57 the anterior teeth and increasing the functional surface area of the molars for the mastication of resistant  
58 foods, while maintaining compressive forces at the temporomandibular joints during both anterior and  
59 postcanine loading [9]. Other studies have rejected the ADLH outright [10].

60 Similarly, the argument that the Neanderthal face incorporates adaptation to life in cold climates  
61 through an improved capacity to condition cold, dry, inspired air also remains controversial. The  
62 proposition that their large nasal cavities would have served to warm and humidify cold air more  
63 effectively [5] has been difficult to test quantitatively [11, 12]. The hypothesis that their well-developed

64 paranasal sinuses [13] are a cold-adaptation has also been questioned. Some have asserted that  
65 Neanderthal paranasal sinuses are not particularly large [14], others have argued that paranasal size is  
66 largely irrelevant in the conditioning of inspired air [15]. Recent studies based on modern human  
67 samples have concluded that it is the shape, not the size of the nasal cavity, that primarily determines  
68 the capacity to warm and humidify inspired air [16]. It has been proposed that airway size likely relates  
69 to the energetics of the organism, whereas airway shape might be more indicative of physiology and  
70 climate [17].

71 A third hypothesis that might in part explain Neanderthal facial morphology is that it represents  
72 adaptation to facilitate greater ventilatory demands driven by high energy expenditures [18, 19]. High  
73 respiratory demands have been proposed for Neanderthals and other 'archaic' humans, such as *H.*  
74 *heidelbergensis*, based on evidence for relatively high body masses and routinely strenuous  
75 hunting/foraging behaviours [20]. Regarding Neanderthals, selective pressure may have been further  
76 increased by high cold resistance costs [21] as well as energetic hunting strategies [22].

77 Although considerable effort has been expended on addressing these explanations for Neanderthal  
78 facial morphology no extensive quantification of facial stressor strain regimes during biting have been  
79 performed. Regarding the modelling of heat transfer and humidification, CFD has previously been  
80 applied in vertebrate palaeontology and to some extant hominids [23, 24]. Most recently two modern  
81 humans have been compared to a partial model of a Neanderthal nasal passage [25]. Results showed  
82 that the partial Neanderthal was less efficient at conditioning cold, dry air than a modern north-eastern  
83 Asian, but slightly more efficient than a southern European. However, unlike the present study, this  
84 previous study only incorporated differences in external nasal aperture and the Neanderthal's internal  
85 nasal passage was not reconstructed. Moreover, no previous CFD analyses have included modelling of  
86 a close outgroup to modern humans and Neanderthals, or compared respiratory flow rates, meaning  
87 that CFD results have yet to be placed in a broader evolutionary context.

88 The application of quantitative 2D beam theory to craniofacial biomechanics represents a major  
89 advance over qualitative general comparisons, but 3D computer-based approaches, such as FEA, allow  
90 the biomechanics of whole structures to be analysed and compared based on a range of performance  
91 metrics [26-28]. In recent years FEA has been increasingly applied in palaeoanthropology [26, 29-32],  
92 boosted by improvements in virtual reconstruction methodologies (figure 1) and integration with

93 geometric morphometrics (GMM) [33-35]. Importantly, FEA also allows the researcher to directly predict  
94 mechanical performance in great detail and compare it in comparative contexts [26]. Similarly, while  
95 CFD is a time-consuming process which limits sample sizes, it is the only means available that allows  
96 researchers to directly test the effects of geometry on fluid and heat flow in living and extinct taxa,  
97 whereas morphometric-based approaches are restricted to identifying correlations between morphology  
98 and variables such as diet or climate [24].

99

100

## 101 **2. Material and methods**

102

103 **Materials.** Models are based on computed tomography of the following specimens: Broken Hill 1, Mauer  
104 1 (*Homo heidelbergensis*); La Ferrassie 1, La Chapelle-aux-Saints 1, Gibraltar 1, Le Moustier 1,  
105 Regourdou 1 (*H. neanderthalensis*); Mladeč 1 (Pleistocene *Homo sapiens*); NMB 1271 Khoe-San  
106 female, ULAC210 European male; AMNH 99/7889 Asian female, PM 0003 Asian male, AMNH 19.33  
107 European female, AMNH 99.1/511 Inuit male, PM 1702, Inuit female, DO.P.004 European male, PM  
108 1532 Pacific male, PM 0084 Peruvian female, UNC002 European male, and UNC013 African American  
109 male (recent *Homo sapiens*).

110 These latter two modern human specimens (CFD analyses only) were chosen because they  
111 represented a more polar-adapted (European) and more tropical (African) adapted nasal morphologies  
112 [16, 36].

113 Broken Hill 1 was selected as our outgroup because it is the most complete specimen commonly  
114 assigned to *H. heidelbergensis* [37]. Our selection of Neanderthal material was based on completeness.  
115 Remaining modern human specimens reflected the widest ethnographic range available.

116

### 117 **Virtual reconstructions.**

118 Fossil specimens were variably damaged or fragmentary. Where morphology was missing or damaged  
119 on one side of a specimen, but complete on the other, virtual reconstruction (step 1) was relatively  
120 straightforward [38] ([Electronic Supplementary Material \(figure 3, ESM\) figure S1](#)), i.e., for Broken Hill 1  
121 and Mladeč 1. In all three Neanderthals at least some bone, including internal portions of the nasal

4

122 cavities are damaged or missing altogether. For these, a second step, 'warping', was applied after step  
123 1 reconstruction, following established protocols [33, 39] (figure 1 & figures S2-S4 in ~~Electronic~~  
124 ~~Supplementary Material (ESM)~~). The source mesh for warping was a recent modern *Homo sapiens*  
125 chosen for its particularly regular and symmetrical internal nasal morphology (ULAC-210).

126

127

## 128 **Finite element analyses.**

129 **Model generation.** For our FEA, 3D volume meshes were generated and loads applied on the basis of  
130 computed tomography, largely using previously described protocols [26, 29, 40, 41]. Segmentation was  
131 conducted in Mimics v17 (Materialise) and Finite element models (FEMs) were generated in 3-matic v8  
132 (Materialise) based on a previously described approach [26, 41]. FEMs were kept at ~2 million tet4  
133 elements and assigned a homogeneous property set [40]. Results can be influenced by differences in  
134 the distribution of materials [31, 42] and proportions of cortical and cancellous bone may vary across  
135 large size ranges [43]. However, size differences are not great between specimens included in the  
136 present study and the assignment of multiple properties would have introduced further assumptions ~~for~~  
137 ~~fossil material~~.

138

139 **Muscle forces and constraints.** Application of jaw adductor muscle forces followed published  
140 protocols [29, 40]. Forces were based on muscle physiological cross-sectional area (PCSA) [44],  
141 corrected for pennation and gape [45], such that  $1 \text{ cm}^2 = 30 \text{ N}$  [46]. Muscle forces were scaled on the  
142 basis of cranial volume to the two thirds power [40, 47] and applied using Boneload [48]. Traction were  
143 applied to plate elements modelled as 3D membrane (thickness = 0.0001 mm;  $E = 20.6 \text{ GPa}$ ). We  
144 subjected all models to: a bilateral anterior tooth bite applied to the left and right incisors and canines, a  
145 unilateral anterior tooth bite at the left  $I^1$ , and a unilateral molar bite at the left  $M^2$ . Models were oriented  
146 and constrained following previous methods [40].

147

148 **Automated collection of FEA results.** Comparison of the VM micro-strain at 203 landmarks for each  
149 of the models in this study results in an expected 3,045 individual landmark cases. To automate the  
150 process, a function was developed ~~in Matlab to access Strand7 (v2.4) results via the application~~

151 ~~programming interface (API) allowing for the to~~ rapidly extraction of micro-strain results ~~for any number~~  
152 ~~of landmarks.~~

153

### 154 **Computational Fluid Dynamics.**

155 ~~[24]. Our reconstructions of the Neanderthal nasal passage alone were based on warps using 103~~  
156 ~~landmarks.~~ We used La Chapelle-aux-Saints 1 because it had the most complete nasal passage among  
157 Neanderthals. Assumptions remain of course and accuracy will ultimately be tested by the discovery of  
158 complete Neanderthal crania. However, our reconstruction and CFD clearly shows that the internal  
159 morphology of the Neanderthal nasal passage is very different to that of any of the modern humans  
160 modelled (including ULCA210, the warp source), or Broken Hill 1 (figure 3).

161 Estimated energy savings were calculated for a single breath in each species. We also calculated  
162 maximal airflow through the nasal passages prior to the onset of extensive turbulence through the nasal  
163 passage (and see ESM). For the three modern humans, body masses were obtained directly for  
164 UNC002 and UNC013 [36] and predicted for ULCA210 [49]. For the two extinct *Homo* body masses  
165 were obtained from previous estimates [20]. Using DICOM data and the 3D analytical program, Avizo,  
166 we generated digital casts of the left nasal passage in each of the three modern humans. The soft-  
167 tissue airway of UNC013 was used as a template for soft-tissue nasal passage shape in La Chapelle-  
168 aux-Saints 1 and Broken Hill 1, as well as ULAC210 (see ESM for further detail on soft-tissue  
169 reconstruction which follows previous methods [24]). Fluid dynamic analysis was run using Fluent  
170 (ANSYS Inc, PA).

171 Heat and moisture transfer were simulated for the CNP (figure S7), as the fleshy nasal vestibule is  
172 not preserved in either extinct hominin species. We used a mixed-species model to simulate water  
173 vapour transport and account for relative humidity within the nasal passage and surrounding air  
174 following previously established protocols [50]. Models were run under the widely accepted flow rate of  
175 100 ml/s for one side of the nasal passage [51, 52] (Table S4). A second, mass-dependent flow rate  
176 was also tested (Table S5). We simulated 0°C air at 20% relative humidity. Nasal mucosa of the CNP  
177 was 37°C and assigned 100% relative humidity. CFD results are given in figure 5 and see ESM.

178

### 179 **3. Results and discussion**

180 **FEA**

181 We solved three load cases, comparing von Mises (VM) micro-strain generated in a: 1) bilateral anterior  
182 bite restrained at all upper incisors and canines [4], 2) a unilateral anterior bite restrained at the left  
183 upper first incisor [9], and, 3) a unilateral bite restrained at the left upper second molar for each of our 15  
184 finite element models (FEMs) (figure 2, ESM figures 3 & 4). Muscle forces (ESM Table S1) were scaled  
185 to cranial volume following a  $2/3$  power rule [29, 40]. VM micro-strain was analysed from 203  
186 homologous craniofacial landmarks grouped into 24 curves and 16 surfaces (ESM figures [S3](#) & [S4](#)).  
187 Bite reaction forces, mechanical advantage and reaction forces at the temporomandibular joints were  
188 also computed (ESM Table S1).

189 From FEA of both bilateral and unilateral anterior biting Broken Hill 1 (*H. heidelbergensis*) exhibited  
190 the least mean micro-strain for all facial landmark groups (ESM figures S3 & S7). Statistical  
191 comparisons between the mean recent modern *H. sapiens* and mean *H. neanderthalensis* (ESM figure  
192 S3) revealed few significant differences. Where differences were found, the mean Neanderthal typically  
193 showed lower micro-strain than the mean recent modern human, however, in most instances one or  
194 more recent modern humans fell within the Neanderthal range (figure S7). The late Pleistocene modern  
195 human, Mladeč 1, fell within or below the Neanderthal range in almost all instances (ESM figures S3 &  
196 S7).

197 In unilateral anterior biting mechanical advantage was consistently higher in modern humans (mean  
198 = 0.37) than in any of the Neanderthals (mean = 0.32), which in turn recorded slightly higher mechanical  
199 advantage than *H. heidelbergensis* (0.29). This is reflected in the bite reaction forces (BRF) at the  
200 anterior teeth in loadings where muscle forces were scaled to the volume<sup>2/3</sup> of bone in the cranium. In  
201 *Homo heidelbergensis* (Broken Hill 1), which exhibited the highest cranial volume and muscle forces,  
202 BRF was 428 Newtons (N), above either the mean (371 N) or any individual result for the three  
203 Neanderthals. However, the distinction was less clear compared to the modern human sample, which,  
204 despite much lower muscle forces (70% that of Broken Hill 1) recorded a mean of 399 N.

205 Our predictions of mechanical performance during a unilateral bite at  $M^2$  revealed even fewer  
206 significant differences in micro-strain between the mean recent modern human and mean Neanderthal  
207 ([ESM figure S4](#)). Mechanical advantage in molar biting is slightly lower for Broken Hill 1 (0.48) than for  
208 the mean Neanderthal (0.50), although within the Neanderthal range ([ESM Table S1](#)). For all modern

209 humans mechanical advantage (mean = 0.67) is well above that of either Broken Hill 1 or any of the  
210 Neanderthals (Table 1). Again this is reflected in the  $M^2$  bite reaction force data. BRF at  $M^2$  for Broken  
211 Hill 1 (719 N) was above either the mean or any individual BRF at  $M^2$  for the three Neanderthals (Mean  
212 = 581 N). While, despite much lower muscle forces, mean BRF at  $M^2$  for modern humans (719 N) was  
213 identical to that computed for Broken Hill 1 and four of the modern humans generated higher BRFs at  
214  $M^2$  than did Broken Hill 1 (ESM Table S1).

215 Considered together with the VM micro-strain results, we find no clear support for the argument that  
216 the facial morphology of Neanderthals is an adaptation linked to heavy anterior biting. Although we  
217 found that Neanderthals have higher average mechanical advantage in biting at the anterior teeth than  
218 Broken Hill 1, differences were minor and micro-strain was relatively high in the Neanderthals, despite  
219 higher bite reaction forces in *H. heidelbergensis*. In unilateral biting at  $M^2$  *H. heidelbergensis* fell within  
220 the Neanderthal range for mechanical advantage, but again generated higher bite reaction forces while  
221 exhibiting less micro-strain.

222 TMJ reaction forces were uniformly in tension in unilateral  $M^2$  biting for the modern humans,  
223 suggesting that they cannot exert maximal muscle forces concurrently on working and balancing sides  
224 in biting at  $M^2$  without generating distractive forces on the working side [53, 54]. The functional  
225 significance of this remains uncertain because a relatively modest reduction in muscle force on the  
226 balancing side brings the working side back into compression, with only slight reduction to bite reaction  
227 force [54]. Working-to-balancing-side asymmetry in muscle recruitment is commonly observed in  
228 primates [55].

229 | There is an interesting potential trade-off in unilateral molar biting, in that increased mechanical  
230 efficiency allows a more powerful bite reaction force for any given muscle force, and, a reduced need for  
231 heavy supporting structures for any given BRF [26], but beyond the point at which the balancing side  
232 TMJ goes into tension some reduction in muscle recruitment and hence reduction in bite reaction force  
233 is required. The real cost of this increased mechanical efficiency in modern humans might be a loss of  
234 available molar occlusal area rather than reduced bite force. The potential benefit is a reduction in the  
235 musculature, bone and energy required.

236

237 **CFD**

238 It is important to note that the modern European (ULCA210) used to generate the source CFD mesh in  
239 our Neanderthal reconstruction, behaved in all respects most like the other ethnic European (UNC002)  
240 and was very distinct from either the Neanderthal or Broken Hill 1 (~~see~~ figure 35).

241 All three species effectively conditioned inspired air. However, modern humans were the most  
242 efficient, recovering 84–96% of energy used. The La Chapelle-aux-Saints 1 nasal passage was 8-10%  
243 less effective than those of the modern humans, and Broken Hill 1 was the least efficient (5–15% and  
244 9.5–25% less efficient than La Chapelle-aux-Saints 1 and the modern humans respectively) (figure 3  
245 and Tables S3–S4). Our CFD results are not necessarily inconsistent with recently published data for a  
246 Neanderthal and two modern humans [25], but cannot be directly compared because of differences in  
247 material and approach. Notably the previous results were based analyses which only considered the  
248 external morphology of the nasal passage. The ensuing model based on 11 landmarks did not address  
249 internal nasal passage geometry. Our Neanderthal model nasal passage was based on a ‘warp’ which  
250 included 103 landmarks, 54 of which were internal landmarks. Previous studies have shown that using a  
251 higher number of landmarks across warped source models will produce more accurate target models  
252 [39, 56].

253 At 18,723 mm<sup>3</sup>, the reconstructed Neanderthal nasal passage was ~29% larger than the average  
254 volume of the modern humans (14,487 mm<sup>3</sup>), which were in turn considerably greater than that of  
255 Broken Hill 1 (11,751 mm<sup>3</sup>). However, total volume of the nasal passage is not the sole predictor of  
256 maximal airflow rates, which are also influenced by the interaction of lung tidal volume, breathing  
257 frequency, and the calibre of the conducting portion of the respiratory system. In humans, the size of the  
258 nostril and nasal valve are the strongest determinants of flow rate limits. Although smaller calibre air  
259 spaces are found deeper in the nasal passage (e.g., the olfactory slit / superior meatus), their effect on  
260 flow rate can be offset by larger calibre openings located within the same cross sectional plane, allowing  
261 more air to pass by without requiring excessive air speeds to maintain continuity. In contrast, all inspired  
262 air must pass through the nostril and choana, making these the prime choke points for airflow within the  
263 nasal passage. As the nostril is the smaller of the two openings, it will impose a greater limit on airflow.  
264 Based on predicted nostril sizes for La Chapelle-aux-Saints 1 and Broken Hill 1 (see ESM), our CFD  
265 analyses predicted that the Neanderthal could move almost twice the volume of air through their nasal  
266 passages under laminar conditions than modern humans (~50 Litres/minute (L/m) in Neanderthal vs

267 ~27 L/m in modern humans). Despite its lower total nasal volume, predicted nostril size in Broken Hill 1  
268 (see ESM) gave a maximum airflow rate of ~42 L/m, lower than for the Neanderthal, but still  
269 substantially higher than in the modern humans.

270 Our results indicate that nasal passage shape, rather than total nasal cavity size, is the critical factor  
271 here (and see ESM). Results are in agreement with the proposition that Neanderthals, and to a lesser  
272 extent, Broken Hill 1, may have had considerably higher energetic demands than modern humans, a  
273 finding consistent with predictions of both Neanderthal and *H. heidelbergensis* physiology [20, 21, 57]  
274 and lung volume [58]. A further point to consider is that this capacity to move more air through the nasal  
275 cavity would have conferred a higher nasal to oral breathing threshold on Neanderthals, allowing them  
276 to benefit from the air conditioning and pathogen/pollutant filtering capacity [59] of the nose over a wider  
277 range of flow rates than other human species.

278

#### 279 **4. Conclusions.**

280 Our results show that, compared to either the likely more 'primitive' condition in *H. heidelbergensis*, or  
281 the independently derived condition in modern humans, Neanderthals are not clearly better-adapted to  
282 sustain high loads on the anterior teeth and Hypothesis 1 is rejected. However, relative to the likely  
283 pleisiomorphic condition, Neanderthal nasal passage morphology may represent an adaptation to cold  
284 that improves conditioning of inspired air, albeit a less efficient solution to that found in modern humans.  
285 These findings are consistent with Hypothesis 2. Our results further suggest that the Neanderthal  
286 capacity to move greater air volumes than either Broken Hill 1, or modern humans, may also represent  
287 an adaptation to cold, insofar as it could support a cold climate physiology [57]. An alternative, not  
288 mutually exclusive explanation, is that this ability reflects an adaptation to a more strenuous,  
289 energetically demanding lifestyle demanding high calorific intakes. It has been calculated that  
290 Neanderthals used 3,360 to 4,480 kcal per day to support winter foraging and cold resistance [21].  
291 Consequently we conclude that Hypothesis 3 is also supported and that the distinctive facial  
292 morphology of Neanderthals has been driven, at least in part, by adaptation to cold, both regarding the  
293 conditioning of inspired air and a greater ventilatory capacity demanded by cold resistance.

294

295 **Ethics.** Research conducted for this study was largely performed on skeletal and fossil specimens that are  
296 repositied in accredited museums. The protocols for collection and use of scans for UNC013 and UNC002 were  
297 reviewed and approved by the Duke University and University of North Carolina Institutional Review Boards. IRB  
298 numbers are DUMC IRB 4881-03 and UNC-CH IRB 03-Surg-372.

299  
300 **Data accessibility.** All data, code and results needed to replicate this study are available from Dryad  
301 [doi:10.5061/dryad.39272]. Additional results and supplemental methods have been uploaded as part of the  
302 electronic supplementary material (ESM). CT scan data is repositied with the museums/institutes that hold  
303 copyright; requests to use scan data should be made directly to those museums/institutes.

304  
305 **Author Contributions.** S.W. & W.C.H.P. conceived and developed experimental design. W.C.H.P. generated  
306 'warps' for virtual reconstructions. W.C.H.P., J.L., J.B. & S.W. conducted analyses. S.W., W.C.H.P., J.L., J.B.,  
307 S.P.E., L.F., S.B., J.J.H., C.S., O.K., M.C., T.C.R. & T.K. contributed data. S.W. wrote the MS with contributions  
308 from all other authors. To whom correspondence should be addressed. E-mail: S.W. (swroe@une.edu.au) or  
309 W.C.H.P. (w.parr@unsw.edu.au).

310  
311 **Funding.** Research was supported by an Australian Research Council Discovery Grant DP140102659 to S.W.,  
312 W.C.H.P., & L.F.

313  
314 **Acknowledgements.** We thank Almut Hoffmann (Museum für Vor und Frühgeschichte, Berlin) and Andreas  
315 Winzer (Department of Human Evolution, MPI) for access to fossil material, and three anonymous reviewers as  
316 well as editorial staff for feedback.

317

## 318 **References**

- 319 [1] Trinkaus, E. 1987 The Neandertal face: evolutionary and functional perspectives on a recent hominid face. *J.*  
320 *Human Evol.* **16**, 429-443.  
321 [2] Franciscus, R.G. 1999 Neandertal nasal structures and upper respiratory tract "specialization.". *Proc. Natl.*  
322 *Acad. Sci. USA* **96**, 1805-1809.  
323 [3] Trinkaus, E. 2003 Neandertal faces were not long; modern human faces are short. *Proc. Natl. Acad. Sci. U.S.A.*  
324 **100**, 8142-8145. (doi:10.1073/pnas.1433023100).  
325 [4] Rak, Y. 1986 The Neanderthal: a new look at an old face. *J. Human Evol.* **15**, 151-164.  
326 [5] Coon, C.S. 1962 *The origin of races*. New York, Knopf.  
327 [6] Weaver, T.D. 2009 The meaning of Neandertal skeletal morphology. *Proc. Natl. Acad. Sci. U.S.A.* **106**, 16028-  
328 16033. (doi:10.1073/pnas.0903864106).  
329 [7] Clement, A.F., Hillson, S.W. & Aiello, L.C. 2012 Tooth wear, Neanderthal facial morphology and the anterior  
330 dental loading hypothesis. *J. Human Evol.* **62**, 367-376. (doi:<http://dx.doi.org/10.1016/j.jhevol.2011.11.014>).

- 331 [8] Demes, B. 1987 Another look at an old face: biomechanics of the neandertal facial skeleton reconsidered. *J.*  
332 *Human Evol.* **16**, 297-303.
- 333 [9] Spencer, M.A. & Demes, B. 1993 Biomechanical analysis of masticatory system configuration in Neandertals  
334 and Inuits. *Am. J. Phys. Anthropol.* **91**, 1-20. (doi:10.1002/ajpa.1330910102).
- 335 [10] O'Connor, C.F., Franciscus, R.G. & Holton, N.E. 2005 Bite force production capability and efficiency in  
336 neanderthals and modern humans. *Am. J. Phys. Anthropol.* **127**, 129-151.
- 337 [11] Maddux, S.D., Butaric, L.N., Yokley, T.R. & Franciscus, R.G. 2017 Ecogeographic variation across  
338 morphofunctional units of the human nose. *Am. J. Phys. Anthropol.* **162**, 103-119. (doi:10.1002/ajpa.23100).
- 339 [12] Maddux, S.D., Yokley, T.R., Svoma, B.M. & Franciscus, R.G. 2016 Absolute humidity and the human nose: A  
340 reanalysis of climate zones and their influence on nasal form and function. *Am. J. Phys. Anthropol.* **161**, 309-320.  
341 (doi:10.1002/ajpa.23032).
- 342 [13] Churchill, S. 1998 Cold adaptation, heterochrony, and neanderthals. *Evol. Anthr.* **7**, 46-61.
- 343 [14] Rae, T., Koppe, T. & Stringer, C.B. 2011 The Neanderthal face is not cold-adapted. *J. Human Evol.* **60**, 234-  
344 239.
- 345 [15] Holton, N.E., Yokley, T.R. & Franciscus, R.G. 2011 Climatic adaptation and Neandertal facial evolution: A  
346 comment on Rae et al. (2011). *J. Human Evol.* **61**, 624-627. (doi:<http://dx.doi.org/10.1016/j.jhevol.2011.08.001>).
- 347 [16] Holton, N., Yokley, T. & Butaric, L. 2013 The Morphological Interaction Between the Nasal Cavity and  
348 Maxillary Sinuses in Living Humans. *Anat. Rec.* **296**, 414-426. (doi:10.1002/ar.22655).
- 349 [17] Bastir, M. & Rosas, A. 2013 Cranial airways and the integration between the inner and outer facial skeleton  
350 in humans. *Am. J. Phys. Anthropol.* **152**, 287-293. (doi:10.1002/ajpa.22359).
- 351 [18] Jelinek, A.J. 1994 Hominids, Energy, Environment, and Behavior in the Late Pleistocene. In *Origins of*  
352 *Anatomically Modern Humans* (eds. M.H. Nitecki & D.V. Nitecki), pp. 67-92. Boston, MA, Springer US.
- 353 [19] Churchill, S.E. 2014 Surviving the Cold. In *Thin on the Ground* (pp. 107-150, John Wiley & Sons, Inc.
- 354 [20] Froehle A.W., Y.T.R., Churchill S. E. 2013 Energetics and the origin of modern humans. In *The Origins of*  
355 *Modern Humans: Biology Reconsidered* (ed. A.J.C.M. Smith F. H.), pp. 285-320. Hoboken, Wiley-Blackwell.
- 356 [21] Steegmann, A.T., Cerny, F.J. & Holliday, T.W. 2002 Neandertal cold adaptation: Physiological and energetic  
357 factors. *Am. J. Hum. Biol.* **14**, 566-583. (doi:10.1002/ajhb.10070).
- 358 [22] Berger, T.D. & Trinkaus, E. 1995 Patterns of Trauma among the Neandertals. *Journal of Archaeological*  
359 *Science* **22**, 841-852. (doi:[https://doi.org/10.1016/0305-4403\(95\)90013-6](https://doi.org/10.1016/0305-4403(95)90013-6)).
- 360 [23] Nishimura, T., Mori, F., Hanida, S., Kumahata, K., Ishikawa, S., Samarat, K., Miyabe-Nishiwaki, T., Hayashi, M.,  
361 Tomonaga, M., Suzuki, J., et al. 2016 Impaired Air Conditioning within the Nasal Cavity in Flat-Faced *Homo*. *PLoS*  
362 *Comput. Biol.* **12**, e1004807. (doi:10.1371/journal.pcbi.1004807).
- 363 [24] Bourke, J.M., Ruger Porter, W.M., Ridgely, R.C., Lyson, T.R., Schachner, E.R., Bell, P.R. & Witmer, L.M. 2014  
364 Breathing Life Into Dinosaurs: Tackling Challenges of Soft-Tissue Restoration and Nasal Airflow in Extinct Species.  
365 *Anat. Rec.* **297**, 2148-2186. (doi:10.1002/ar.23046).
- 366 [25] de Azevedo, S., González, M.F., Cintas, C., Ramallo, V., Quinto-Sánchez, M., Márquez, F., Hünemeier, T.,  
367 Paschetta, C., Ruderman, A., Navarro, P., et al. 2017 Nasal airflow simulations suggest convergent adaptation in  
368 Neanderthals and modern humans. *Proceedings of the National Academy of Sciences*.  
369 (doi:10.1073/pnas.1703790114).
- 370 [26] Wroe, S., Ferrara, T.L., McHenry, C.R., Curnoe, D. & Chamoli, U. 2010 The craniomandibular mechanics of  
371 being human. *Proc. R. Soc. Lond. [Biol.]* **277**, 3579-3586.
- 372 [27] Rayfield, E.J. 2007 Finite Element Analysis and Understanding the Biomechanics and Evolution of Living and  
373 Fossil Organisms. *Annu. Rev. Earth Planet. Sci.* **35**, 541-576.
- 374 [28] Dumont, E.R., Piccirillo, J. & Grosse, I.R. 2005 Finite-element analysis of biting behavior and bone stress in  
375 the facial skeletons of bats. *The Anatomical Record Part A* **283A**, 319-330.
- 376 [29] Ledogar, J.A., Smith, A.L., Benazzi, S., Weber, G.W., Spencer, M.A., Carlson, K.B., McNulty, K.P., Dechow, P.C.,  
377 Grosse, I.R., Ross, C.F., et al. 2016 Mechanical evidence that *Australopithecus sediba* was limited in its ability to  
378 eat hard foods. *Nat. Commun.* **7**. (doi:10.1038/ncomms10596).
- 379 [30] Strait, D.S., Weber, G.W., Neubauer, S., Chalk, J., Richmond, B.G., Lucas, P.W., Spencer, M.A., Schrein, C.,  
380 Dechow, P.C., Ross, C.F., et al. 2009 The feeding biomechanics and dietary ecology of *Australopithecus africanus*.  
381 *Proc. Natl. Acad. Sci. U.S.A.* **106**, 2124-2129.
- 382 [31] Wroe, S., Moreno, K., Clausen, P., McHenry, C. & Curnoe, D. 2007 High resolution three-dimensional  
383 computer simulation of hominid cranial mechanics. *Anat. Rec.* **290**, 1248-1255.

- 384 [32] Ledogar, J.A., Benazzi, S., Smith, A.L., Weber, G.W., Carlson, K.B., Dechow, P.C., Grosse, I.R., Ross, C.F.,  
385 Richmond, B.G., Wright, B.W., et al. 2017 The Biomechanics of Bony Facial “Buttresses” in South African  
386 Australopiths: An Experimental Study Using Finite Element Analysis. *Anat. Rec.* **300**, 171-195.  
387 (doi:10.1002/ar.23492).
- 388 [33] Parr, W., Wroe, S., Chamoli, U., Richards, H.S., McCurry, M., Clause, P.D. & McHenry, C.R. 2012 Toward  
389 integration of geometric morphometrics and computational biomechanics: New methods for 3D virtual  
390 reconstruction and quantitative analysis of Finite Element Models. *Journal of Theoretical Biology* **301**, 1-14.
- 391 [34] O'Higgins, P., Cobb, S.N., Fitton, L.C., Groning, F., Phillips, R., Liu, J. & Fagan, M.J. 2011 Combining geometric  
392 morphometrics and functional simulation: an emerging toolkit for virtual functional analyses. *J. Anat.* **218**, 3-15.
- 393 [35] Smith, A.L., Benazzi, S., Ledogar, J.A., Tamvada, K., Smith, L.C.P., Weber, G.W., Spencer, M.A., Dechow, P.C.,  
394 Grosse, I.R., Ross, C.F., et al. 2015 Biomechanical implications of intraspecific shape variation in chimpanzee  
395 crania: moving towards an integration of geometric morphometrics and finite element analysis. *Anatomical  
396 record (Hoboken, N.J. : 2007)* **298**, 122-144. (doi:10.1002/ar.23074).
- 397 [36] Yokley, T.R. 2009 Ecogeographic variation in human nasal passages. *Am. J. Phys. Anthropol.* **138**, 11-22.  
398 (doi:10.1002/ajpa.20893).
- 399 [37] Mounier, A. & Mirazón Lahr, M. 2016 Virtual ancestor reconstruction: Revealing the ancestor of modern  
400 humans and Neandertals. *J. Human Evol.* **91**, 57-72. (doi:<https://doi.org/10.1016/j.jhevol.2015.11.002>).
- 401 [38] Senck, S., Coquerelle, M., Weber, G.W. & Benazzi, S. 2013 Virtual Reconstruction of Very Large Skull Defects  
402 Featuring Partly and Completely Missing Midsagittal Planes. *Anat. Rec.* **296**, 745–758. (doi:10.1002/ar.22693).
- 403 [39] Gunz, P., Mitteroecker, P., Neubauer, S., Weber, G.W. & Bookstein, F.L. 2009 Principles for the virtual  
404 reconstruction of hominin crania. *J. Human Evol.* **57**, 48-62.
- 405 [40] Ledogar, J.A., Dechow, P.C., Wang, Q., Gharpure, P.H., Gordon, A.D., Baab, K.L., Smith, A.L., Weber, G.W.,  
406 Grosse, I.R., Ross, C.F., et al. 2016 Human feeding biomechanics: performance, variation, and functional  
407 constraints. *PeerJ* **4**, e2242. (doi:10.7717/peerj.2242).
- 408 [41] McHenry, C.R., Wroe, S., Clausen, P.D., Moreno, K. & Cunningham, E. 2007 Supermodeled sabercat,  
409 predatory behavior in *Smilodon fatalis* revealed by high-resolution 3D computer simulation. *Proc. Natl. Acad. Sci.  
410 U.S.A.* **104**, 16010-16015.
- 411 [42] Strait, D.S., Wang, Q., Dechow, P.C., Ross, C.F., Richmond, B.G., Spencer, M.A. & Patel, B.A. 2005 Modeling  
412 elastic properties in finite-element analysis: How much precision is needed to produce an accurate model? *Anat.  
413 Rec.* **283A**, 275-287.
- 414 [43] Chamoli, U. & Wroe, S. 2011 Allometry in the distribution of material properties and geometry of the felid  
415 skull: Why larger species may need to change and how they may achieve it. *Journal of Theoretical Biology* **283**,  
416 217-226. (doi:10.1016/j.jtbi.2011.05.020).
- 417 [44] van Eijden, T.M.G.J., Korfage, J.A.M. & Brugman, P. 1997 Architecture of the human jaw-closing and jaw-  
418 opening muscles. *Anat. Rec.* **248**, 464-474. (doi:10.1002/(SICI)1097-0185(199707)248:3<464::AID-AR20>3.0.CO;2-  
419 M).
- 420 [45] Taylor, A.B. & Vinyard, C.J. 2013 The relationships among jaw-muscle fiber architecture, jaw morphology,  
421 and feeding behavior in extant apes and modern humans. *Am. J. Phys. Anthropol.* **151**, 120-134.  
422 (doi:10.1002/ajpa.22260).
- 423 [46] Murphy, R.A. 1998 Skeletal muscle. In *Physiology* (eds. R.M. Berne & M.N. Levy), p. 294. St Louis, Mosby.
- 424 [47] Strait, D.S., Grosse, I.R., Dechow, P.C., Smith, A.L., Wang, Q., Weber, G.W., Neubauer, S., Slice, D.E., Chalk, J.,  
425 Richmond, B.G., et al. 2010 The Structural Rigidity of the Cranium of *Australopithecus africanus*: Implications for  
426 Diet, Dietary Adaptations, and the Allometry of Feeding Biomechanics. *The Anatomical Record: Advances in  
427 Integrative Anatomy and Evolutionary Biology* **293**, 583-593.
- 428 [48] Grosse, I.R., Dumont, E.R., Coletta, C. & Tolleson, A. 2007 Techniques for modeling muscle-Induced forces in  
429 finite element models of skeletal structures. *Anat. Rec.* **290**, 1069-1088.
- 430 [49] Kappelman, J. 1996 The evolution of body mass and relative brain size in fossil hominids. *J. Human Evol.* **30**,  
431 243-276. (doi:<https://doi.org/10.1006/jhevol.1996.0021>).
- 432 [50] Naftali, S., Rosenfeld, M., Wolf, M. & Elad, D. 2005 The air-conditioning capacity of the human nose. *Ann  
433 Biomed Eng* **33**. (doi:10.1007/s10439-005-2513-4).
- 434 [51] Doorly, D.J., Taylor, D.J., Gambaruto, A.M., Schroter, R.C. & Tolley, N. 2008 Nasal architecture: form and  
435 flow. *Philos. Trans. Roy. Soc. London Ser. A* **366**, 3225-3246. (doi:10.1098/rsta.2008.0083).

- 436 [52] Weinhold, I. 2004 Numerical Simulation of Airflow in the Human Nose. *Eur. Arch. Otorhinolaryngol.* **261**, 452-  
437 455.
- 438 [53] Greaves, W.S. 1978 The jaw lever system in ungulates: a new model. *J Zool Lond* **184**, 271–285.
- 439 [54] Clausen, P., Wroe, S., McHenry, C., Moreno, K. & Bourke, J. 2008 The vector of jaw muscle force as  
440 determined by computer-generated three dimensional simulation: A test of Greaves' model. *J. Biomech.* **41**,  
441 3184-3188.
- 442 [55] Hylander, W.L., Ravosa, M.J., Ross, C.F. 2004 Jaw muscle recruitment patterns during mastication in  
443 anthropoids and prosimians. In *Shaping primate evolution* (ed. F. Anapol, German, R.Z., Jablonski N.J.), pp. 229–  
444 257. Cambridge, Cambridge University Press.
- 445 [56] Parr, W.C.H., Wroe, S., Chamoli, U., Richards, H.S., McCurry, M.R., Clausen, P.D. & McHenry, C. 2012 Toward  
446 integration of geometric morphometrics and computational biomechanics: New methods for 3D virtual  
447 reconstruction and quantitative analysis of Finite Element Models. *Journal of Theoretical Biology* **301**, 1-14.  
448 (doi:<http://dx.doi.org/10.1016/j.jtbi.2012.01.030>).
- 449 [57] Fiorenza, L., Benazzi, S., Henry, A., Salazar-García, D.C., Blasco, R., Picin, A., Wroe, S. & Kullmer, O. 2015 To  
450 meat or not to meat? New perspectives on Neanderthal ecology. *Am. J. Phys. Anthropol.* **156**, (S59) 43-71.
- 451 [58] Weinstein, K.J. 2008 Thoracic morphology in Near Eastern Neandertals and early modern humans compared  
452 with recent modern humans from high and low altitudes. *J. Human Evol.* **54**, 287-295.  
453 (doi:<http://dx.doi.org/10.1016/j.jhevol.2007.08.010>).
- 454 [59] White, D.E., Bartley, J. & Nates, R.J. 2015 Model demonstrates functional purpose of the nasal cycle. *Biomed.*  
455 *Eng. Online* **14**, 1-11. (doi:10.1186/s12938-015-0034-4).

456

457 **Figure captions**

458 **Figure 1.** La Chapelle-aux-Saints 1 Neanderthal mesh-mesh metric comparison of initial fossil material (A) with  
459 final reconstruction (B) (performed in Cloud Compare). The models are superimposed (C) and the original-  
460 reconstructed mesh-mesh metrics are computed. Regions where the final reconstruction lies further out (from the  
461 model centroid) than the original fossil material are shown in blue. Regions where the final reconstruction lies  
462 further in (from the model centroid) than the original fossil material are shown in red. Regions of the original fossil  
463 material that lie further than +/- 1.875 mm (3 voxel edge lengths) from the final reconstruction have been clipped  
464 from the image. Regions that overlap almost exactly are shown in off-white.

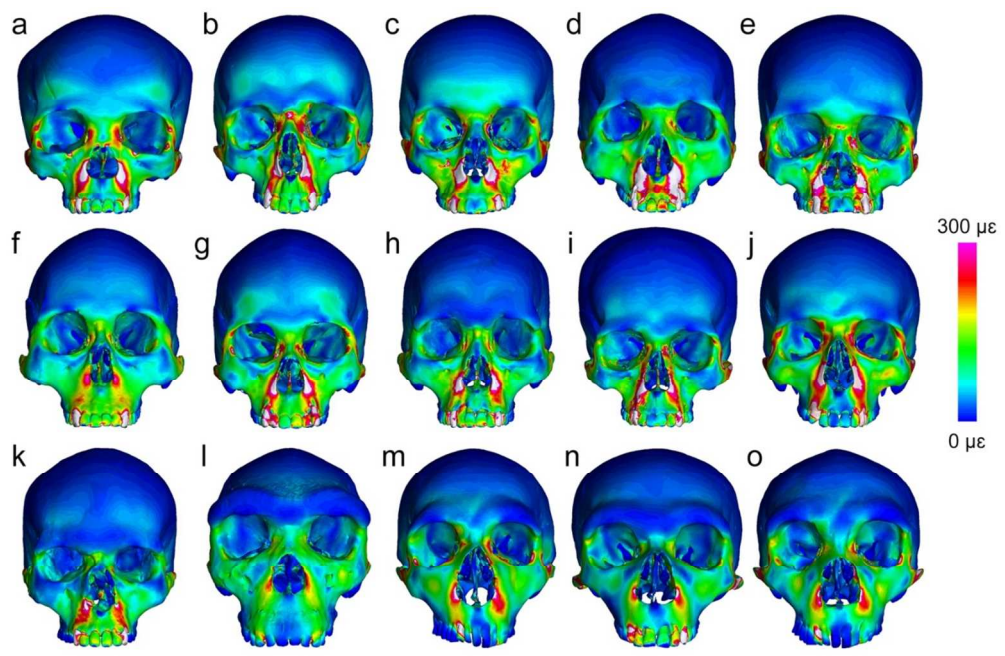
465

466 **Figure 2.** Results of Finite Element Analysis under an anterior bite simulation (loading via muscle force scaled to  
467 volume<sup>2/3</sup>, restraints applied to incisors and canines) for ten recent (A-J) and one Pleistocene (K) modern human,  
468 as well as *H. heidelbergensis* (L), and three *H. neanderthalensis* (M-O). Number of elements for each models also  
469 given for: A) Khoe-San female, 1,571,213, B) Caucasian male, 1,602,686, C) European female, 1,651,738, D)  
470 Chinese male, 1,593,342, E) Malay female, 1,608,934, F) Inuit male, 1,625,463, G) Inuit female, 1,700,708, H)  
471 Pacific Islander male, 1,701,642, I) Peruvian female, 1,619,268, J) European male, 1,651,945, K) Mladeč 1,  
472 1,724,664, L) Broken Hill 1, 1,611,994, M) La Ferrassie 1, 1,618,373, N) La Chapelle-aux-Saints 1, 1,625,022, and  
473 O) Gibraltar 1, 1,609,723.

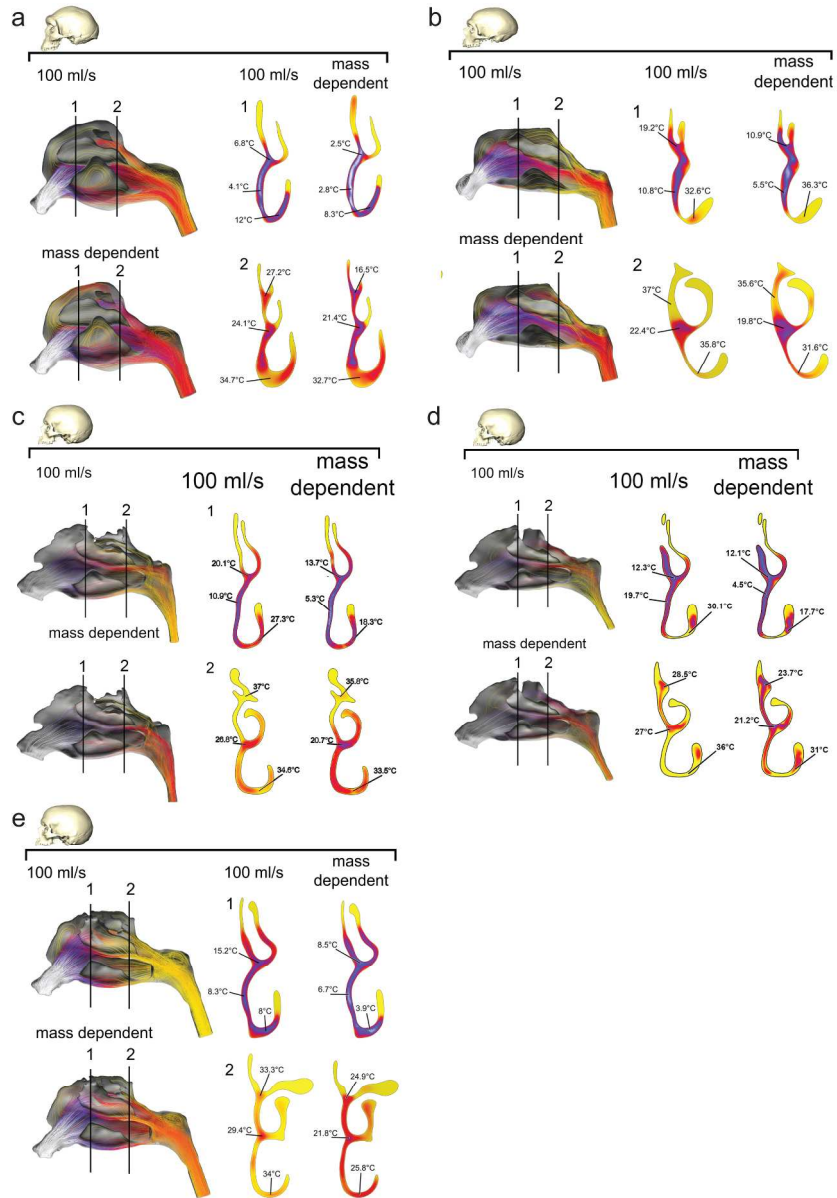
474

475 **Figure 3.** Figure 5. Heat flow through the left nasal passage of a (A) *Homo heidelbergensis*, (B) *Homo*  
476 *neanderthalensis*, and (C) *Homo sapiens* (UNC002). (D) *Homo sapiens* (ULAC210). (E) *Homo sapiens* (UNC013).  
477 Heat transfer is shown in cross sections taken at numbered regions in each nasal passage, and shown under both  
478 100 ml/s and the mass-dependent flow rate.  
479





156x102mm (220 x 220 DPI)



207x295mm (300 x 300 DPI)